RESEARCH ARTICLE

ADVANCED OPTICAL MATERIALS

www.advopticalmat.de

Anti Stokes Thermometry of Plasmonic Nanoparticle Arrays

Simone Ezendam, Lin Nan, Ianina L. Violi, Stefan A. Maier, Emiliano Cortés, Guillaume Baffou,* and Julian Gargiulo**

Metallic nanoparticles possess strong photothermal responses, especially when illuminated as ensembles due to collective effects. However, accurately quantifying the temperature increase remains a significant challenge, impeding progress in several applications. Anti Stokes thermometry offers a promising solution by enabling direct and non-invasive temperature measurements of the metal without the need for labeling or prior calibration. While Anti Stokes thermometry is successfully applied to individual nanoparticles, its potential to study light-to-heat conversion with plasmonic ensembles remains unexplored. In this study, the theoretical framework and the conditions that must be fulfilled for applying Anti Stokes thermometry to ensembles of nanoparticles are discussed. Then, this technique is implemented to measure the light-induced heating of square arrays of Au nanodisks. The obtained temperature measurements are validated using wavefront microscopy, demonstrating excellent agreement between the two thermometry methods. These results showcase the extension of Anti Stokes thermometry to plasmonic ensembles, highlighting its potential for implementation in the diverse photothermal applications involving these systems.

1. Introduction

Metallic nanoparticles (NPs) exhibit localized surface plasmon resonances that significantly enhance their interaction with light.[1] They are powerful harvesters of the energy of incoming photons, that is concentrated in subwavelength regions,[2] giving rise to numerous applications.[3] Because part of the energy is confined inside the lossy metal, the use of plasmonic NPs is inevitably accompanied by heating.[4] Depending on the application, this can constitute an undesirable side effect or can be harnessed as a powerful quality to exploit.[5–7] While the generation of heat with plasmonic NPs is an unavoidable process, its accurate quantification remains a significant challenge, hindering progress in multiple fields. For instance, precise control of the released heat is essential in implementing hyperthermia therapies in medicine,[8,9] or remote drug release.[10,11] Additionally, temperature measurements are important in fields aiming to quantitatively model and control thermally induced processes, such as thermally driven nanofluidics.[12,13] Furthermore, some fields struggle to understand the interplay between thermal and non-thermal effects, such as in plasmon-assisted catalysis[14–17] or optical trapping.[18–20] In all these situations, achieving temperature measurements under *in operando* conditions using non-invasive techniques remains a key challenge.

Numerous experimental thermometry techniques have been proposed for plasmonics.[21,22] These techniques primarily involve quantifying a temperature-dependent property, such as the

S. Ezendam, L. Nan, S. A. Maier, E. Cortés, J. Gargiulo
Nanoinstitute Munich
Faculty of Physics
Ludwig-Maximilians-Universität
80539 München, Germany
E-mail: emiliano.cortes@lmu.de; jgargiulo@unsam.edu.ar

The ORCID identification number(s) for the author(s) of this article can be found under https://doi.org/10.1002/adom.202301496

DOI: 10.1002/adom.202301496

I. L. Violi
Instituto de Nanosistemas
Universidad Nacional de San Martín
San Martín, Buenos Aires 1650, Argentina

S. A. Maier
School of Physics and Astronomy
Monash University
Clayton 3800, Australia

S. A. Maier
Department of Physics
Imperial College London
London SW7 2AZ, UK

G. Baffou
Institut Fresnel
CNRS
Aix Marseille Univ
Centrale Marseille, Marseille 13013, France
E-mail: guillaume.baffou@fresnel.fr

fluorescence (intensity, spectrum, polarization, lifetime),[23] Raman (intensity, spectrum),[24,25] phase transition,[12,26] viscosity,[27] or binding-time[28,29] of a nearby probe in close proximity to the nanosystem. However, these techniques require previous calibrations of the probes and yield a temperature that is not necessarily the same as the NP. In addition, wavefront microscopy[30–32] can be used to map temperature distributions around heated NPs immersed in a liquid, with diffraction-limited resolution, by probing the wavefront distortion created by the temperature-induced variation of the refractive index of the liquid.[32]

More recently, an emerging method called Anti Stokes (AS) thermometry offers promising solutions for measuring the temperature of plasmonic NPs themselves. The method capitalizes on the temperature-dependent behavior of the AS photoluminescence (PL) emission spectrum of the plasmonic material when illuminated by a continuous-wave laser. AS thermometry is non-invasive, label-free, and does not require any additional characterization or prior knowledge of the NPs or the properties of the medium.[22,33]. AS thermometry was first introduced by Xi and Cahill in 2016 and demonstrated single-particle sensitivity using Au nanodisks.[34] Since then, it has mostly been applied to individual NPS of different shapes (such as Au rods,[35,36] bowties,[37] spheres,[33,38] and stars,[39] and Au core – Pd shell and Au core-Pd satellites[40]) supported on glass substrates and in air or water environments. However, isolated NPs represent only a limited scope of plasmonic applications. In numerous scenarios, multiple NPs are simultaneously illuminated.[41] AS thermometry on gold NPs ensembles has also been performed.[34,37,42] However, in these cases, the NPs just acted as probes and their plasmonic properties did not contribute to the heating process. In these previous reports, the temperature of the sample was controlled either via the employment of a thermal stage or by means of a cryostat. Here, we explore a different heating aspect of NPs arrays. In our study, the heating of NP ensembles is light-induced, offering the possibility to evidence and study photothermal collective effects that can give rise to significant enhancements in their photothermal response compared to isolated NPs.[43,44] To avoid confusions and make a clear difference between these two approaches, we shall occasionally speak about photothermal AS thermometry in the following to emphasize that, in our approach, heating is light-induced. Developing photothermal AS thermometry is useful for many emerging applications of plasmonic ensembles, such as photothermal catalysis,[17,45] micro-optical devices,[46] microfluidics,[47] or the development of anti-fogging surfaces.[48]

In this work, we demonstrate the implementation of AS thermometry for light-induced heating of plasmonic ensembles and validate the temperature measurements using wavefront microscopy. First, we introduce a theoretical formalism for photothermal AS thermometry of ensembles and discuss its range of validity. In addition, we provide guidelines on how to optimize its practical implementation to maximize PL signals. Applying the developed formalism and guidelines, AS thermometry is employed to study periodic square arrays of different-sized Au nanodisks. Subsequently, we utilize wavefront microscopy on the same samples, under identical illumination conditions and using the same microscope. This enables a direct comparison between the two methods, and their high level of agreement enhances confidence in both techniques. These results constitute the extension of photothermal AS thermometry to plasmonic ensembles.

2. Results

2.1. From One to Many Nanoparticles in AS Thermometry

In this section, we discuss the conditions to use AS thermometry for ensembles of NPs. We limit the discussion to the case where both heating and probing are performed with the same excitation laser at irradiance I_{exc} and wavelength λ_{exc}. For an individual NP, the AS $I^{AS}(\lambda, \lambda_{exc}, T)$ and Stokes $I^{S}(\lambda, \lambda_{exc})$ PL emission intensity at wavelength λ are given by:[33]

$$I^{AS}(\lambda, \lambda_{exc}, T) \propto f_I(I_{exc}) f_{PL}(\lambda, \lambda_{exc}) n(\lambda, \lambda_{exc}, T) \tag{1a}$$

$$I^{S}(\lambda, \lambda_{exc}) \propto f_I(I_{exc}) f_{PL}(\lambda, \lambda_{exc}) \tag{1b}$$

Here, f_I describes the dependence of the signal intensity on the excitation irradiance I_{exc}, f_{PL} is the intrinsic PL spectrum, and $n(\lambda, \lambda_{exc}, T)$ is the temperature-dependent distribution of the states that provide the extra energy for AS emission. For an ensemble of nanoparticles, the total signal is the sum of the individual signals:

$$I_N^{AS}(\lambda, \lambda_{exc}, T) \propto \sum_k^N f_{I,k}(I_{exc}) f_{PL,k}(\lambda, \lambda_{exc}) n(\lambda, \lambda_{exc}, T_k) \tag{2a}$$

$$I_N^{S}(\lambda, \lambda_{exc}, T) \propto \sum_k^N f_{I,k}(I_{exc}) f_{PL,k}(\lambda, \lambda_{exc}) \tag{2b}$$

Here, $f_{I,k}$ and $f_{PL,k}$ are the intensity dependence and the intrinsic PL of particle k, T_k is the temperature of particle k, and N is the number of emitting NPs. In the following, we assume that all particles have the same dependence on intensity $f(I_{exc})$, which is reasonable given that PL emission scales linearly with the excitation irradiance.[49–52] In addition, we consider the case where all NPs are at the same temperature. Then, $f(I_{exc})$ and $n(\lambda, \lambda_{exc}, T)$ can be taken out of the summation.

$$I_N^{AS}(\lambda, \lambda_{exc}, T) \propto f(I_{exc}) n(\lambda, \lambda_{exc}, T) \left(\sum_k^N f_{PL,k}(\lambda, \lambda_{exc}) \right) \tag{3a}$$

$$I_N^{S}(\lambda, \lambda_{exc}, T) \propto f(I_{exc}) \left(\sum_k^N f_{PL,k}(\lambda, \lambda_{exc}) \right) \tag{3b}$$

Extracting the temperature of the system from Equation (3) is challenging as it requires knowledge of the emission properties of each NP in the summation term. Instead, the ratios Q_{i,j_N}^{AS} and Q_{i,j_N}^{S} between the PL spectra of the ensemble measured at two different excitation irradiances $I_{exc,i}$ and $I_{exc,j}$ can be calculated so that the terms with the summations are canceled out.

$$Q_{i,j_N}^{AS} = Q_{i,j_N}^{S} \frac{n(\lambda, \lambda_{exc}, T_i)}{n(\lambda, \lambda_{exc}, T_j)}$$
$$Q_{i,j_N}^{S} = \frac{f(I_{exc,i})}{f(I_{exc,j})} \tag{4}$$

In the context of AS thermometry with continuous-wave excitation (CW), a Bose–Einstein (BE) distribution is used for $n(\lambda, \lambda_{exc}, T_i)$, given by:[33]

$$n(\lambda, \lambda_{exc}, T) = \frac{1}{e^{[E(\lambda)-E(\lambda_{exc})]/k_B T} - 1} \tag{5}$$

Here, k_B is the Boltzmann constant, and T refers indistinctly to the lattice or the electron gas temperature, as differences between the two temperatures are negligible under most experimental conditions with CW illumination.[33] Further discussion on the choice of $n(\lambda, \lambda_{exc}, T)$ can be found in Section S1 Supporting Information. In addition, if the temperature scales linearly with the excitation irradiance, we can introduce the photothermal coefficient β through $T = T_0 + \beta I_{exc}$ where T_0 is the temperature of the system in the absence of light. Finally, combining this with Equations (4) and (5) yields the following expression:

$$Q^{AS}_{i_{j_N}} = Q^{S}_{i_j} \frac{e^{[E(\lambda)-E(\lambda_{exc})]/k_B(T_0+\beta I_{exc,j})} - 1}{e^{[E(\lambda)-E(\lambda_{exc})]/k_B(T_0+\beta I_{exc,i})} - 1} \tag{6}$$

Equation (6) is identical to what has previously been derived for a single NP and has only one unknown parameter, β.[33] This expression can be used for any arrangement of nanoparticles, whether they are identical or not, as long as the condition that the temperature is constant across the collection of nanoparticles is fulfilled.

Because the same laser is used to heat and excite PL, the correlation between the strength of PL signals and the number of NPs in the ensemble is not trivial. Due to collective effects, the ensemble heats more efficiently compared to the isolated NP. This means that lower irradiances are required to achieve the same temperature increase. Unfortunately, the PL signal is proportional to the irradiance, resulting in weaker signals per NP when increasing the number of illuminated NPs at a constant temperature. This could represent a problem for which photothermal AS thermometry could not be extended to many particles. To quantitatively analyze this effect, we define a figure of merit called $F = \frac{P^{PL}}{\Delta T}$ which is given by the ratio of the total emitted PL power P^{PL} to the light-induced temperature increase ΔT under the same illumination conditions. For a single NP, $F^s = 4\pi\phi\bar{\kappa}R_L$, where ϕ is the PL quantum yield, $\bar{\kappa}$ is the averaged thermal conductivity of the surrounding media and R_L is the Laplace radius of the NP (for a detailed derivation of this expression, refer to Section S2, Supporting Information). F provides information on the emitted PL power per increased degree, and it is useful to compare the emission of systems at the same temperature.

For a 2D periodic array, the general dependence of F on the number of illuminated particles N is given by (see Section S2, Supporting Information)

$$F^{2D} \propto \frac{\sqrt{A}}{R_L}\sqrt{N}F^s \tag{7}$$

where A is the area of the unit cell (for a square lattice, $A = p^2$ with p the interparticle distance). This means that moving from one to multiple NPs in AS thermometry at constant temperature makes the signal increase proportional to the square root on the number of NPs, and not to the number of NPs as could have been expected.

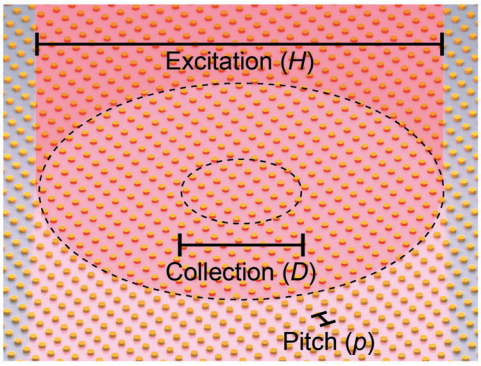

Figure 1. AS thermometry for ensembles of nanoparticles. Illustration of the conditions for measuring collective heating using AS thermometry (not to scale). A collection of NPs in an array with pitch p are excited with a Gaussian beam with a full-width half maximum size H. The collection size D indicates the region from where the PL emission is collected.

In the derivation of Equation (7), it was assumed that the number of illuminated and detected NPs is the same. However, in some experimental cases, it might be necessary to collect the PL signal only from a subset of the illuminated NPs, causing a decrease in the figure of merit. This is the case of the experimental measurements presented in the next section, where we study a square periodic array of identical NPs illuminated by a Gaussian beam with a full-width half maximum size of H and collect the emitted PL signal only from the NPs inside an area of diameter D. A schematic illustrating these parameters is shown in **Figure 1**b. In this particular case, the figure of merit is given by (see Section S2, Supporting Information)

$$F^a = \frac{2\sqrt{\ln 2}\pi\bar{\kappa}D^2\phi}{H} = \frac{D^2}{H}\frac{1}{2\sqrt{\pi}R_L}F^s \tag{8}$$

Equation (8) indicates that in order to maximize PL signals, the collection size D should be as close to H as possible. However, the applicability of AS thermometry as described in Equation (6) is limited to situations where the temperature is uniform within the NPs in the collection area, which imposes an upper bound to D. In summary, the collection size D should be as large as possible to maximize signals, but small enough to minimize temperature variations within that area.

2.2. Experimental Results

2.2.1. Methods, Setup, and Samples Description

Figure 2a shows the experimental setup used for AS thermometry and wavefront imaging of NPs arrays. A lens is used to focus a 647 nm excitation beam at the back focal plane of the objective (water immersion, NA=1.1). This produces a collimated Gaussian beam with $H \approx 18\mu m$ at the sample position that serves both for heating and PL excitation. For AS thermometry, the emitted PL is collected by the same objective and focused on a multimode optical fiber coupled to a spectrometer. The collection size

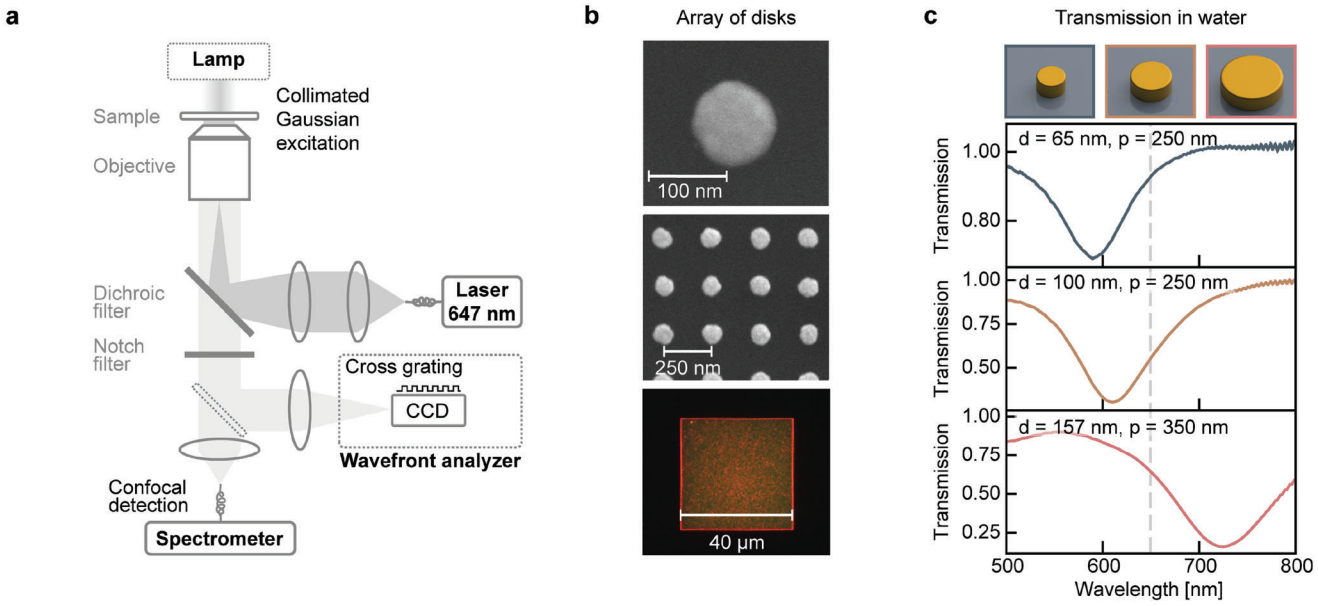

Figure 2. Setup and sample. a) Illustration of the setup. The 647 nm excitation laser is focused on the back focal plane of the objective to achieve collimated Gaussian illumination. The emitted PL is transmitted to a spectrometer after being spatially filtered using a fiber. For wavefront microscopy, a lamp for Köhler illumination is added in transmission and the signal is directed to a wavefront analyzer. b) Scanning electron microscopy images (top and middle) along with a dark-field image (bottom) of a d = 100 nm array. c) Normalized transmission in water of the arrays with three different disk sizes. The dashed vertical line indicates the laser wavelength of 647 nm.

corresponds to $D = 6\mu m$ at the sample plane. For wavefront microscopy, the sample is illuminated with a halogen lamp in a Köhler configuration. The transmitted light is directed to quadriwave lateral shearing interferometry (QLSI) camera, consisting of a CCD camera with a 2D grating separated by a millimetric distance. For both techniques, the laser light is blocked by a notch filter before reaching the detector.

To minimize any potential sources of heterogeneities in the samples and experimental setup, we took temperature measurements with AS thermometry and wavefront microscopy under the same microscope, at the same sample position under the same excitation conditions in the following way: i) The desired excitation irradiance was set, and the microscope was configured as shown in Figure 2a without the components shown in dashed lines. PL emission spectrum was acquired. ii) Without changing the sample position, the laser's shutter was closed, the halogen lamp was turned on, and the detection port was switched to the QLSI camera. A reference wavefront image (without heating) was acquired. iii) The laser shutter was opened, and a second wavefront image was acquired. iv) The process was repeated with a new excitation irradiance value.

For this study, three different square arrays of Au nanodisks were fabricated using electron-beam lithography, named d065, d100, and d157, as shown in Figure 2b,c. The name indicates the diameter of the disks (see Section S3, Supporting Information, for information on the size characterization). The interparticle distances are $p^{d065} = 250$ nm, $p^{d100} = 250$ nm, and $p^{d157} = 350$ nm. All arrays are $40 \times 40\ \mu m^2$ in size, and all disks have a height of 40 nm. Figure 2b shows Scanning Electron Microscopy (SEM) and dark field (DF) images of sample d100. Before the photothermal measurements, the arrays were softly annealed by illuminating them for 2 min at a high irradiance of $I_{max} = 0.156$ mW μm^{-2} with the 647 nm laser beam. It was observed that this process stabilizes the disks under illumination (see Section S4, Supporting Information for further details). Additionally, this illumination is also beneficial to photobleach any residual molecule that could emit PL or fluorescence and contribute to the background. Figure 2c shows the optical transmission of the arrays measured in water, after the photothermal annealing. The vertical dashed line indicates the excitation wavelength used for annealing and AS thermometry.

2.2.2. Photothermal AS Thermometry

PL spectra were measured for the three fabricated arrays. Because the collection area D is three times smaller than the excitation beam size H, the temperature of the NPs within that region can be considered constant.[43] Therefore, their photothermal response can be described by a single photothermal coefficient β. The number of NPs inside the collection area is $N_c^{d065} \approx 450$, $N_c^{d100} \approx 450$ and $N_c^{d157} \approx 230$ for each arrays. It is interesting to calculate the figures of merit under these measuring conditions, as defined by Equation (8). The values are $F^{d065} = 17$, $F^{d100} = 12$ and $F^{d157} = 9$. These numbers indicate that despite having hundreds of emitting NPs inside the collection area, the PL signals are only tens of times larger than a single emitting NP at the same temperature.

Figure 3a displays exemplary PL spectra obtained from a d100 array at four different excitation irradiances. Figure 3b shows examples of the calculated AS Q_{i,j_N}^{AS} and Stokes Q_{i,j_N}^{S} ratios, respectively. The AS ratios were fitted by Equation (6). Because T_0 is the room temperature ($T_0 = 20°C$) and the excitation irradiances are known, the photothermal coefficient β is the only free parameter

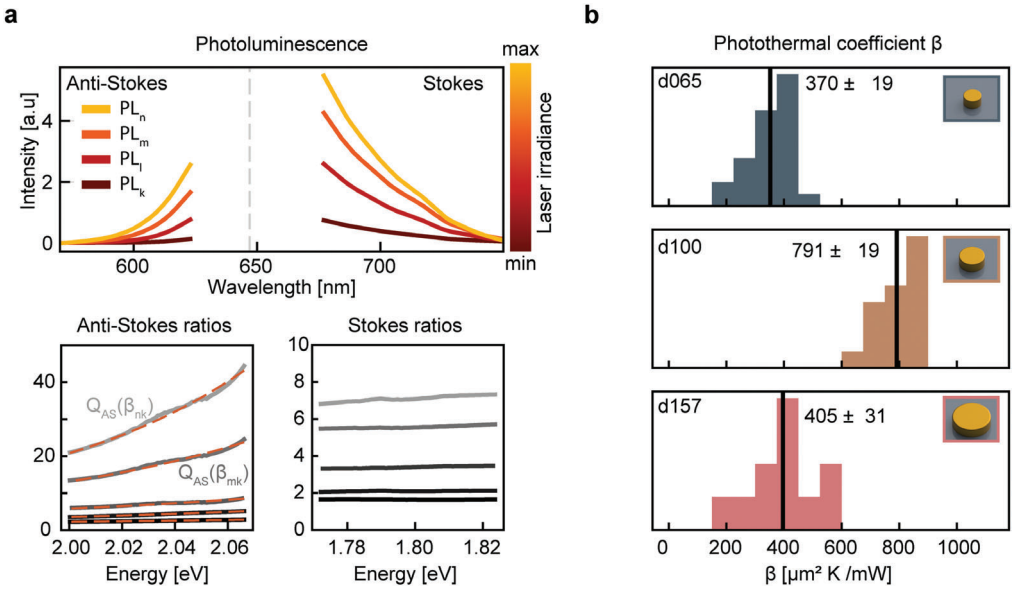

Figure 3. Photothermal measurements. a) PL spectra of the d100 array at four different excitation irradiances. b) EAS and Stokes ratios in solid lines, with the AS fitted for the photothermal coefficient β shown in dashed orange lines. c) Histograms of the photothermal coefficients obtained for the three different disk sizes.

to fit. The dashed lines in Figure 3b indicate the resulting fits. If M different excitation irradiances are used, the number of ratios Q^{AS}_{i,j_N} that can be calculated is $\binom{M}{2}$. We measured the arrays at seven different excitation irradiances, ranging from 0.011 to 0.156 mW μm^{-2} with an integration time of 30 s. This means that β is measured $\binom{7}{2} = 21$ times for each sample. Figure 3c shows the histograms of the obtained values of β for the three different disk sizes. The obtained values were $\beta_{d065} = (370 \pm 19)$ μm^2 K mW^{-1}, $\beta_{100} = (791 \pm 19)$ μm^2 K mW^{-1} and $\beta_{157} = (405 \pm 31)$ μm^2 K mW^{-1}. These values exceed the typical values for isolated NPs by an order of magnitude (see for example Ref. [33] and Section S7 of the Supporting Information), confirming the existence of collective heating. In particular, the d100 array demonstrated the highest photothermal coefficient, which can be attributed to its plasmon resonance being closer to the excitation wavelength, as shown in Figure 2c.

2.2.3. Wavefront Microscopy

Wavefront microscopy was implemented as described in previous reports.[30] For each excitation irradiance of the heating laser, two wavefront images are acquired, with and without the heating beam. The subtraction of these two images gives the wavefront distortion created by the temperature increase in the surrounding water medium, from which a quantitative temperature map of the sample can be calculated. An example of such a map is shown in **Figure 4**a, corresponding to a d100 array at an excitation irradiance of $I_{exc} = 0.156$ mW μm^{-2}.

It must be noted that wavefront microscopy using QLSI is a diffraction-limited technique, and therefore the spatial resolution of the temperature field is ≈300 nm. However, the experimental conditions presented here correspond to a temperature regime known as "delocalized", wherein the temperature varies smoothly in the surrounding medium. In other words, the temperature is smooth throughout the array, even at the microscale, and despite the nanoscale nature of the heat sources. This regime occurs when $\zeta_2 = \frac{p^2}{3HR_L} << 1$ (for more details refer to Ref. [43] and Section S5 of the Supporting Information). For the three arrays under study, $\zeta_2 < 0.04$. This facilitates the comparison between wavefront microscopy and AS thermometry, as it allows the assignment of a single temperature value to the region marked with a black circle in Figure 4a, corresponding to the collection area used for AS thermometry. For each irradiance and each array, we calculated the average $\overline{T}$ and the standard deviation σ_T of the temperature inside that region. Typically, $\frac{\sigma_T}{\overline{T}} \sim 1.5\%$ (see Section S6 of the Supporting Information for details).

2.2.4. Discussion

Figure 4b shows the temperature increase ΔT versus excitation irradiance I_{exc} experimentally determined by both techniques. Solid lines correspond to the median β measured by AS thermometry, and the shaded area shows the range between the 1st and 3rd quantile. The data points in circles are the values determined using wavefront microscopy, with most of the points lying in the shaded area.

In addition, it is illustrative to compare the experimental results with thermal theoretical calculations. For that, we first calculated the absorption and extinction cross-sections of the individual Au disks, shown in Figure 4c (refer to Section S7, Supporting Information for details on the calculations). In the same figure, the wavelengths of minimum transmittance of the arrays from Figure 2c are indicated with vertical solid lines. Evidently, the theory fails to predict the exact position of the plasmon resonances. Then, the theoretical photothermal responses of the

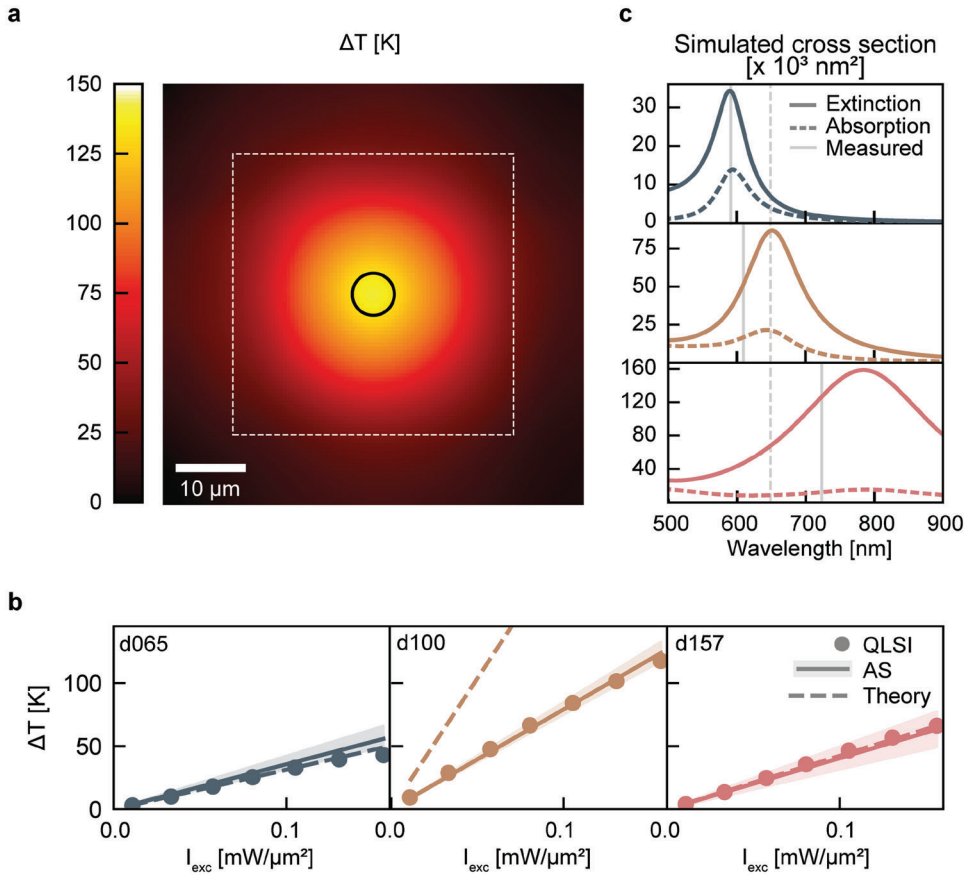

Figure 4. Validation of measured temperatures. a) Exemplary extracted 2D temperature map using wavefront microscopy. The dashed line illustrates the array size, and the black circle corresponds to the collection area for the AS measurements. b) Experimental results of wavefront microscopy and AS thermometry. The solid line shows the temperature increase against maximum irradiance estimated from the median photothermal coefficient β, shaded area shows the 1st and 3rd quantile. Data points show the temperature determined by wavefront microscopy. The dashed line is the calculated temperature increase at the center of the array. c) Optical simulations of the extinction and absorption cross-sections of the disks. The vertical solid lines correspond to the measured transmission minima as presented in Figure 2c. The verticle dashed line indicates the laser wavelength used for heating and PL excitation.

arrays are calculated and shown in dashed lines in 4c (refer to Section S8, Supporting Information for details). The theory significantly overestimates the temperature values for d100, which has the heating wavelength closest to its plasmon resonance. For this reason, any error in predicting the position of the resonance propagates to the calculation of absorption. In contrast, the other two arrays have heating wavelengths far from resonance, where the spectra present smaller slopes and are thus less sensitive to miscalculations. It is not our intention here to fully discuss the source of modeling errors, probably caused by a deviation from a perfect 3D disk shape or a change in the Au degree of crystallinity during the annealing process, as also observed by Osaka and coworkers.[53] On the contrary, the aim is to draw attention to the complexity of quantitative prediction of photothermal responses when complete system information is not available. The complexity mainly resides in the calculation of exact absorption cross-sections and in the setting of the thermal boundary conditions due to the presence of irregular interfaces or the existence of interfacial Kapitza resistances.[37,54] Overall, these complexities highlight the necessity for accurate nanothermometry techniques.

3. Conclusion

In conclusion, we have demonstrated the applicability of photothermal AS thermometry for investigating the collective heating of plasmonic ensembles. We have derived a method to extract the photothermal coefficient β of a group of NPs from the analysis of its PL emission, analogous to what has previously been derived for isolated NPs. Additionally, we have introduced a figure of merit that enables the comparison of PL signals between NP ensembles and their isolated counterparts, taking into account experimental parameters such as the excitation beam size and the collection area. Importantly, the PL signal (at constant temperature) is not proportional to the number N of NPs illuminated and probed, as it is usually the case in metrology. The signal only scales as $\sqrt{N}$. In this regard, the figure of merit proves valuable in the context of AS thermometry as it provides guidelines for optimizing experimental designs and evaluating the feasibility of measurements.

Then, we performed AS thermometry for three different square periodic arrays of varying sizes of Au nanodisks. Specifically, we measured the photothermal coefficient of a group

of a few hundred central NPs within each array. The results obtained with AS thermometry were compared and validated against wavefront microscopy measurements, an independent alternative thermometry method. The comparison revealed a good agreement between the two techniques, which enhances confidence in both approaches. Moreover, this also enhances confidence in AS thermometry for its implementation at the single-particle level, where a comparison with alternative non-invasive techniques is technologically more challenging. It is interesting to note that although both techniques agree with each other, they deviate from theoretical estimations. This emphasizes the challenge of thermal modeling when complete information about the systems is lacking and brings to light the importance of thermometry methods, particularly those capable of operating in complex environments difficult to model.

In this work, we studied the collective heating of an array, and focused on measuring the temperature of a single group of NPs within it. It is worth noting that alternative measurement strategies could be explored in the future, such as moving the position of the collecting fiber (or its image at the sample plane) to target different groups of particles, that is, to obtain a spatial thermal profile. The spatial resolution of this scanning approach will be determined by the size of the collection area at the sample plane. However, a decrease in the collecting area will reduce the collected signal. Again, the figures of merit introduced here (such as the one given by Equation (8)) serve as valuable tools for assessing the limitations of the measurement conditions.

Until now, AS thermometry has mainly been used at the single-particle level. Here, we have shown that it can be extended to ensembles of multiple particles and provided guidelines on how to perform this extension. A crucial aspect is that the method we have presented can also be employed with non-ordered arrays, non-identical particles, or more complex surrounding media. This versatility makes it valuable for the wide range of photothermal applications involving plasmonic ensembles. By showcasing the extension of AS thermometry to such scenarios, we have opened up new possibilities and expanded its potential impact in the field.

Supporting Information

Supporting Information is available from the Wiley Online Library or from the author.

Acknowledgements

The authors acknowledge DFG under e-conversion Germany's Excellence Strategy (Grant no. EXC 2089/1-390776260), the Bavarian program Solar Energies Go Hybrid (SolTech), the Center for NanoScience (CeNS), and the European Research Council (Grant no. 802989 "CATALIGHT"). J.G. acknowledges the AvH Foundation for the Experienced Researcher Fellowship and Agencia I+D+I (Grant PICT-2020-SERIEA-02966).

Open access funding enabled and organized by Projekt DEAL.

Conflict of Interest

The authors declare no conflict of interest.

Data Availability Statement

The data that support the findings of this study are available from the corresponding author upon reasonable request.

Keywords

anti stokes photoluminescence, nanothermometry, photothermal effect, thermoplasmonics

Received: June 23, 2023
Revised: August 14, 2023
Published online:

[1] S. A. Maier, *Plasmonics: Fundamentals and Applications*, Springer, Berlin, Germany **2007**.
[2] V. Giannini, A. I. Fernández-Domínguez, S. C. Heck, S. A. Maier, *Chem. Rev.* **2011**, *111*, 3888.
[3] V. Amendola, R. Pilot, M. Frasconi, O. M. Maragò, M. A. Iatì, *J. Phys.: Condens. Matter* **2017**, *29*, 203002.
[4] J. B. Khurgin, *Nat. Nanotechnol.* **2015**, *10*, 2.
[5] G. Baffou, F. Cichos, R. Quidant, *Applications and Challenges of Thermoplasmonics* **2020**, *19*, 946.
[6] G. Liu, J. Xu, T. Chen, K. Wang, *Phys. Rep.* **2022**, *981*, 1.
[7] X. Cui, Q. Ruan, X. Zhuo, X. Xia, J. Hu, R. Fu, Y. Li, J. Wang, H. Xu, *Chem. Rev.* **2023**, *123*, 6891.
[8] M. R. Ali, I. M. Ibrahim, H. R. Ali, S. A. Selim, M. A. El-Sayed, *Int. J. Nanomed.* **2016**, *11*, 4849.
[9] A. Paściak, R. Marin, L. Abiven, A. Pilch-Wróbel, M. Misiak, W. Xu, K. Prorok, O. Bezkrovnyi, Ł. Marciniak, C. Chanéac, F. Gazeau, R. Bazzi, S. Roux, B. Viana, V.-P. Lehto, D. Jaque, A. Bednarkiewicz, *ACS Appl. Mater. Interfaces* **2022**, *14*, 33555.
[10] M. J. Penelas, C. B. Contreras, P. C. Angelomé, A. Wolosiuk, O. Azzaroni, G. J. Soler-Illia, *Langmuir* **2020**, *36*, 1965.
[11] C. Zhan, W. Wang, J. B. McAlvin, S. Guo, B. P. Timko, C. Santamaria, D. S. Kohane, *Nano Lett.* **2016**, *16*, 177.
[12] M. Fränzl, F. Cichos, *Nat. Commun.* **2022**, *13*, 656.
[13] D. J. Simon, T. Thalheim, F. Cichos, F. Hartmann, *Macromol. Chem. Phys.* **2023**, *224*, 2300060.
[14] L. Zhou, D. F. Swearer, C. Zhang, H. Robatjazi, H. Zhao, L. Henderson, L. Dong, P. Christopher, E. A. Carter, P. Nordlander, N. J. Halas, *Science* **2018**, *362*, 69 LP.
[15] Y. Sivan, J. Baraban, I. W. Un, Y. Dubi, *Science* **2019**, *364*, eaaw9367.
[16] C. Zhan, B. W. Liu, Y. F. Huang, S. Hu, B. Ren, M. Moskovits, Z. Q. Tian, *Nat. Commun.* **2019**, *10*, 2671.
[17] L. Mascaretti, A. Schirato, P. Fornasiero, A. Boltasseva, V. M. Shalaev, A. Alabastri, A. Naldoni, *Nanophotonics* **2022**, *11*, 3035.
[18] Q. Jiang, B. Rogez, J. B. Claude, G. Baffou, J. Wenger, *Nano Lett.* **2020**, *20*, 8811.
[19] J. Gargiulo, T. Brick, I. L. Violi, F. C. Herrera, T. Shibanuma, P. Albella, F. G. Requejo, E. Cortés, S. A. Maier, F. D. Stefani, *Nano Lett.* **2017**, *17*, 5747.
[20] I. L. Violi, L. P. Martinez, M. Barella, C. Zaza, L. Chvátal, P. Zemánek, M. V. Gutiérrez, M. Y. Paredes, A. F. Scarpettini, J. Olmos-Trigo, V. R. Pais, I. D. Nóblega, E. Cortes, J. J. Sáenz, A. V. Bragas, J. Gargiulo, F. D. Stefani, *J. Chem. Phys.* **2022**, *156*, 3.
[21] M. Quintanilla, L. M. Liz-Marzán, *Nanotoday* **2018**, *19*, 126.
[22] G. Baffou, *ACS Nano* **2021**, *15*, 5785.
[23] M. T. Carlson, A. Khan, H. H. Richardson, *Nano Lett.* **2011**, *11*, 1061.
[24] Z. Fang, Y. R. Zhen, O. Neumann, A. Polman, F. J. García De Abajo, P. Nordlander, N. J. Halas, *Nano Lett.* **2013**, *13*, 1736.

[25] P. Li, S. H. C. Askes, P. Rosendo, F. Ariese, C. Ramanan, E. V. Hauff, A. Baldi, *J. Phys. Chem. C* **2023**, *127*, 9690.
[26] P. M. Bendix, S. N. S. Reihani, L. B. Oddershede, *ACS Nano* **2010**, *4*, 2256.
[27] F. Hajizadeh, L. Shao, D. Andrén, P. Johansson, H. Rubinsztein-Dunlop, M. Käll, *Optica* **2017**, *4*, 746.
[28] S. W. Nooteboom, Y. Wang, S. Dey, P. Zijlstra, *Small* **2022**, *18*, 2201602.
[29] P. A. Reinhardt, A. P. Crawford, C. A. West, G. DeLong, S. Link, D. J. Masiello, K. A. Willets, *J. Phys. Chem. B* **2021**, *125*, 12197.
[30] G. Baffou, P. Bon, J. Savatier, J. Polleux, M. Zhu, M. Merlin, H. Rigneault, S. Monneret, *ACS Nano* **2012**, *6*, 2452.
[31] G. Baffou, *J. Phys. D: Appl. Phys.* **2021**, *54*, 29.
[32] G. Baffou, *ACS Photonics* **2023**, *10*, 322.
[33] M. Barella, *ACS Nano* **2021**, *15*, 2458.
[34] X. Xie, D. G. Cahill, *Appl. Phys. Lett.* **2016**, *109*, 183104.
[35] A. Carattino, M. Caldarola, M. Orrit, *Nano Lett.* **2018**, *18*, 874.
[36] Y. Y. Cai, E. Sung, R. Zhang, L. J. Tauzin, J. G. Liu, B. Ostovar, Y. Zhang, W. S. Chang, P. Nordlander, S. Link, *Nano Lett.* **2019**, *19*, 1067.
[37] S. Jones, D. Andrén, P. Karpinski, M. Käll, *ACS Photonics* **2018**, *5*, 2878.
[38] E. Pensa, J. Gargiulo, A. Lauri, S. Schlücker, E. Cortés, S. A. Maier, *Nano Lett.* **2019**, *19*, 1867.
[39] L. P. Martinez, S. Poklepovich-Caride, J. Gargiulo, E. D. Martínez, F. D. Stefani, P. C. Angelomé, I. L. Violi, *Nano Lett.* **2022**, *23*, 2703.
[40] J. Gargiulo, M. Herran, I. L. Violi, A. Sousa-Castillo, L. P. Martinez, S. Ezendam, M. Barella, H. Giesler, R. Grzeschik, S. Schlücker, S. A. Maier, F. D. Stefani, E. Cortés, *Nat. Commun.* **2023**, *14*, 3813.
[41] E. Cortés, F. J. Wendisch, L. Sortino, A. Mancini, S. Ezendam, S. Saris, L. de S. Menezes, A. Tittl, H. Ren, S. A. Maier, *Chem. Rev.* **2022**, *122*, 15082.
[42] J. T. Hugall, J. J. Baumberg, *Nano Lett.* **2015**, *15*, 2600.
[43] G. Baffou, P. Berto, E. Bermúdez Ureña, R. Quidant, S. Monneret, J. Polleux, H. Rigneault, *ACS Nano* **2013**, *7*, 6478.
[44] L. Zundel, K. Malone, L. Cerdán, R. Martínez-Herrero, A. Manjavacas, *ACS Photonics* **2023**, *10*, 274.
[45] J. R. Adleman, D. A. Boyd, D. G. Goodwin, D. Psaltis, *Nano Lett.* **2009**, *9*, 4417.
[46] B. Ciraulo, J. Garcia-Guirado, I. de Miguel, J. Ortega Arroyo, R. Quidant, *Nat. Commun.* **2021**, *12*, 1.
[47] J. S. Donner, J. Morales-Dalmau, I. Alda, R. Marty, R. Quidant, *ACS Photonics* **2015**, *2*, 355.
[48] C. Walker, E. Mitridis, T. Kreiner, H. Eghlidi, T. M. Schutzius, D. Poulikakos, *Nano Lett.* **2019**, *19*, 1595.
[49] Y. Y. Cai, L. J. Tauzin, B. Ostovar, S. Lee, S. Link, *J. Chem. Phys.* **2021**, *155*, 060901.
[50] A. Tcherniak, S. Dominguez-Medina, W. S. Chang, P. Swanglap, L. S. Slaughter, C. F. Landes, S. Link, *J. Phys. Chem. C* **2011**, *115*, 15938.
[51] W. Rao, Q. Li, Y. Wang, T. Li, L. Wu, *ACS Nano* **2015**, *9*, 2783.
[52] Y. Fang, W. S. Chang, B. Willingham, P. Swanglap, S. Dominguez-Medina, S. Link, *ACS Nano* **2012**, *6*, 7177.
[53] N. Osaka, M. Ozawa, T. Matsuyama, K. Wada, K. Okamoto, *Opt. Mater. Express* **2023**, *13*, 1504.
[54] N. Shenogina, R. Godawat, P. Keblinski, S. Garde, *Phys. Rev. Lett.* **2009**, *102*, 156101.